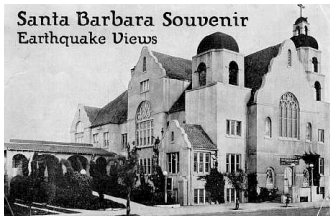

4th IASPEI / IAEE International Symposium:

Effects of Surface Geology on Seismic Motion

August 23–26, 2011 · University of California Santa Barbara

BROADBAND GROUND-MOTIONS FROM RUPTURE DYNAMICS

P. Martin MAI
Division of Physical Sciences Engineering
King Abdullah University of Science & Technology
Thuwal, 23955-6900
Saudi Arabia

Luis A. DALGUER
Swiss Seismological Service
ETH-Zurich
Zurich, CH-8092
Switzerland

ABSTRACT

Simulating realistic broadband ground-motions for earthquake engineering applications is a key challenge in earthquake seismology. This paper describes and applies a method to compute fully physics-based near-field synthetic seismograms in a wide frequency band. We combine spontaneous dynamic rupture modeling with a high-frequency seismic-scattering approach to compute broadband (up to ~50 Hz) seismograms on a dense near-source receiver grid. Our modeling considers buried and surface-rupturing faults on which strike-slip, normal-faulting, and reverse-motion scenario earthquakes occur, embedded in a layered velocity-density model with constant or depth-dependent normal stress. Each earthquake is characterized by an initial random stress field that generates a realistically complex rupture evolution, including heterogeneous slip and variable rise time (slip-rate function). The dynamic rupture calculations return the low-frequency (f ~ 3Hz) radiated seismic waves that we then combine with a high-frequency scattered seismic wavefield to form hybrid broadband seismograms. We calculate the scattered wavefield using multiple backward-S-to-S scattering theory; the resulting high-frequency seismograms are then combined with the dynamic low-frequency waveforms as described in Mai et al. (2010). The scattering parameters are chosen based on previous studies on seismic coda properties, and then calibrated against ground-motion prediction equations. We apply our method for dynamic broadband ground-motion simulations to a large number of M_w 6.5-7.0 scenario earthquakes of different faulting styles, in the vicinity of a critical energy facility whose seismic hazard needs to be re-evaluated. The set of scenario ruptures generates a wide range of ground-shaking behavior. Comparing against modern ground-motion prediction equations, we find (i) larger ground-motion variability but comparable median values; (ii) cases for extreme ground-motions; (iii) surprising reduction in shaking levels in the very near-field of the rupture (R < 5 km). Our results demonstrate the applicability of our methodology for simulation-based seismic hazard assessment, and reveal the need to carefully reconsider ground-motion uncertainty in the near-field of moderate-to-large earthquakes.

INTRODUCTION

Broadband (0 – 20Hz) ground-motion simulation for earthquake-engineering and seismic-hazard purposes is one of the key research topics in earthquake seismology. At the same time, it is one of the most challenging problems, because in general, one needs to simultaneously consider the complexity of the earthquake rupture process, the intricacies of seismic wave-propagation through heterogeneous Earth structure as well as shaking (de-)amplifications due to local site effects. Each of these physical phenomena represents its own research field; creating "end-to-end" simulations that include all three of the fields for realistic ground-motion prediction is thus a difficult task. In this context, we discriminate between ground-motion simulations and ground-motion prediction. While the former attempt to create realistic time series of ground-shaking at selected sites over a generally limited frequency range, the latter employ empirical ground-motion prediction equations (GMPE's) to calculate a few indicative ground-motion parameters (like peak-ground acceleration, PGA, peak-ground velocity, PGV, and spectral acceleration at selected periods, SA_T). While simulation approaches suffer from limiting assumptions in the modeling setup (for the rupture process and Earth structure) and are computationally more expensive, they have the advantage of being in principle more realistic; they also provide full time histories that are needed in nonlinear structural analysis. In contrast, GMPE's are simple to apply, but insufficient for nonlinear structural analysis. For adequate prediction of near-source ground motion seismic hazard analysis, GMPE's suffer from hard-to-quantify variability and

not-well-understood saturation effects at close distance. These deficiencies arise because GMPE's are derived from sparse recorded data, and cannot fully capture effects of complex rupture processes, wave-propagation in heterogeneous Earth, and local site amplification. Accurate physics-based numerical models that contain realistic earthquake source complexity and wave-propagation in 3D Earth are thus needed to correctly assess the level and variability of near-source ground motions.

Many recent damaging crustal earthquakes exhibited very large (often unexpected) ground-accelerations that frequently exceed 1g, as for instances observed in the 2008 M_w 6.9 Iwate-Miyagi Nairiku, Japan earthquake, the 2010 M_w7.0 Darfield, New Zealand event; the 2011 M_w 6.3 Christchurch, New Zealand, earthquake, among others. Besides very large shaking levels in the frequency range of engineering interest (up to 10 Hz), large motions were also observed at relatively low frequencies ~1.0Hz (e.g. in the 2011 M_w 6.3 Christchurch earthquake). An additional observation is that the spatial ground-motion variability is very high, as for instance manifested in the 2004 M_w 6.0 Parkfield earthquake where shaking levels over 1g were observed very close to other sites that only showed moderate shaking levels (Shakal et al, 2006). As summarized by Mai (2009), the variability of recent ground-motion observations often exceeds the ground-motion variability predicted by current GMPE's. Additionally, the saturation effects at very close distances have been questioned, where GMPE's "flatten out" and remain at essentially constant shaking levels at distances less then ~5 km from the fault, owing to advanced numerical simulation results (e.g. Guatteri et al, 2003; Ripperger et al, 2008) and recent observations that indicate that very near-field shaking may in fact decrease (on average) compared to current GMPE's.

The above introduction illustrates the need for advanced broadband ground-motion simulations that account for complexity in the source, scattering in seismic wave propagation, and local site-amplification effects, to better explain and reproduce recent observations on the level and variability of near-field ground motions. The present study comprises dynamic rupture modeling and hybrid broadband ground-motion calculations, focusing on combining low-frequency ($f < 3$ Hz) seismograms that contain the signature of realistically complicated source with high-frequency seismograms that capture scattering effects along the path from the source to the bedrock site. We do not consider local site effects (site amplification or nonlinear site response) in the present study.

METHODS

Dynamic rupture modeling

The details of our dynamic rupture calculations are given in Dalguer and Mai (2011, this volume), and are only briefly summarized here. We assume a fractal initial stress distribution on the rupture plane that is embedded in a one-dimensional velocity-density structure. One suite of simulations assumes constant normal stress, an alternative set utilizes depth-dependent normal stress. We adopt a linear slip-weakening model with constant slip-weakening distance in the center of the fault, increasing to larger values in a 3-km wide buffer zone at the fault boundaries to ensure smooth rupture stopping. We consider ruptures that remain buried (top edge of rupture at 5km depth), and events that are allowed to break the surface. Because the potential faulting-style for these scenario events is not known a priori, we consider a vertical strike-slip rupture plane, a 60°-dipping normal fault, and a 45°-dipping reverse fault. Since we generate 30 realizations of initial stress (parameterized in terms of von Karman correlation function) for each case, we simulate a total of 360 spontaneous dynamic ruptures. The target (maximum) source dimensions follow source-scaling relations (Mai & Beroza, 2000; Wells & Coppersmith, 1994). The complete dynamic rupture calculations thus provide fully physics-based finite-fault rupture models with spatial heterogeneity in the kinematic source parameters slip, slip-velocity, and rupture time; from the dynamic rupture simulations we then extract low-frequency (f_{max} ~3 Hz) seismograms at a dense station array.

Broadband ground-motion simulations

To generate broadband time series for engineering purposes, comprising the frequency range up to ~50 Hz, several methods have been devised in the recent past in which an "arbitrary" stochastic high-frequency (HF) signal is added to pre-computed low-frequency (LF) wavefield. This addition is carried out either in the time-domain (Berge et al, 1998) or in the frequency domain (Graves and Pitarka, 2004) at some pre-selected and fixed matching frequency. However, in these calculations, the phase-angles of the waveforms are not considered. Owing also to a spectral-amplitude mismatch between the LF and HF signal at the fixed matching frequency, the resulting broadband signal are often found to be "energy-deficient" around the matching frequency (Cornell, pers. communication, 2000). What that essentially means is that the building response at corresponding periods, computed from such simulated broadband seismograms, is often inconsistent with the one computed from actual data.

Mai and Beroza (2003) proposed a hybrid broadband ground-motion computation scheme in which the matching frequency for the LF and HF signal is found through an optimization that minimizes both the amplitude and phase mismatch between the two signals. The optimization is carried out within a narrow frequency range (0.1 – 0.2 Hz) around a target matching frequency. The matching thus depends on the individual LF- and HF-time series, and may be different for each component of motion.

For computing the HF-frequency wavefield, we refrain from using "standard" engineering tools to generate stochastic point-source accelerograms (e.g. Boore, 1983). Instead, we compute elementary scattering "Greens functions" utilizing the multiple-scattering theory of Zeng (1991) and Zeng et al. (1993). These scattering wavelets are then convolved with a moment-rate function representing the temporal rupture evolution; following the work of Mena et al. (2010), we use the source-time function described by Dreger et al. (2007). These site-specific scattering operators are then used to form the HF-signal for each station (Mai et al, 2010). Performing the frequency-domain combination of the HF- and LF-signals finally provides simulated broadband seismic signal that are characterized by self-consistent physics both in the rupture process (dominating the long-period motions) and wave-propagation in heterogeneous media (high-frequency scattering).

In the present study, we use scattering parameters according to the work of Edwards et al. (2009). Q_0 is assumed to represent the average crustal attenuation (Anderson and Hough 1984); based on Edwards et al. (2009) we choose $Q_0 = 1300$. We select the corresponding site-kappa as $\kappa = 0.01$, in agreement with the site-specific kappa-values inferred at the site of interest (Edwards et al., 2009). The elastic-wave scattering parameter η_S is selected to be 0.03, representing a mean-free path-length of ~30 km. However, the final ground-motion results are not very sensitive to the particular choice of η_S, as reported by Mena et al. (2010). Additionally, we apply a generic site-amplification function (Borcherdt 1994, 2002) to account for the fact that the dynamic simulations consider a minimum shear-wave speed of 2500 m/s, which is not representative for strong-motion recordings and ground-motion prediction equations derived from strong-motion data. We apply site-amplification function for a minimum shear-wave speed of 1500 m/s. From our dynamically consistent broadband ground-motion simulations we then obtain synthetic seismograms for which ground-motion parameters of interest (PGA, PGV, SA at various periods T) are compared against several recent ground-motion prediction equations.

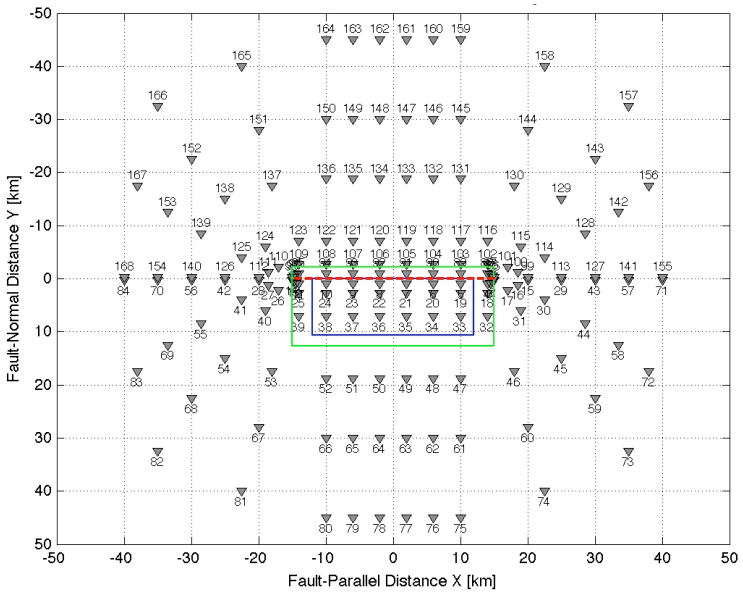

Figure 1: Station and fault geometry for broadband ground-motion simulations. The thick red-line marks the vertical projection of the top-edge of the targeted rupture plane (outlined in blue), the green dotted lines the vertical projection of maximum allowed fault plane.

We compute ground-motions on a virtual receiver array that is arranged around the fault as shown in Figure 1. Due to symmetry, we only consider one half of the plane in case of the strike-slip events. For dipping faults there are 168 stations, for the strike-slip case correspondingly 84 stations, in a distance range $0 \leq R_{JB} \leq 80$ km. Several stations are close to being nodal for the S-wave radiation pattern for the strike-slip earthquakes. For the sites with fault-normal position Y being 1 km or less, the wave-amplitudes on the fault-parallel-component of motion is very small, while all the seismically radiated energy is concentrated on fault-normal-component of motion and the vertical component.

Broadband ground-motions synthetics are generated with 48sec duration, N = 16'384 points, and a sampling of dt = 0.0029294. The nominal maximum frequency of the broadband seismograms is 100 Hz, but we the reliable frequency range extends only to ~50 Hz. As seen in then waveform examples in Figure 2 and 3, the amplitude-spectral decay falls off more rapidly than the expected 1/f (in velocity) beyond f_{max} ~50 Hz due to numerical inaccuracies at the highest frequencies.

The spectral decay of the recorded seismic waves at high frequencies can be described by the expression $A(f) = A_0 \exp[-\pi \kappa f]$, where A_0 is the reference amplitude, f is frequency, and the spectral decay parameters κ is site-kappa. Generally, κ is smaller on rock sites,

and higher on alluvium sites, i.e. low κ mean more efficient propagation of high-frequency seismic energy. In our study, we test several site-kappa values in the vicinity of the results of Edwards et al. (2009) who performed a detailed kappa-study close to the site of interest. Their κ-values fall in the general range $\kappa = 0.02 \pm 0.005$. We test $\kappa = 0.01$ and $\kappa = 0.03$ in our broadband computations; since the overall results do not change drastically, we report our findings for $\kappa = 0.01$ only.

To test the sensitivity of the broadband motions to variations in the scattering parameters, we perform multiple broadband-computations for a subset of scenarios. These tests are not meant to define an "optimal" parameter set, but rather to assess the variability of ground-motion amplitudes for changes in the scattering parameters. In particular we varied:

- The elastic scattering coefficient, η_S, in the range $0.01 \leq \eta_S \leq 0.05$
- The average-crustal attenuation, Q_0, in the range $100 \leq Q_0 \leq 0.05$
- The frequency-decay parameter, α, in the range $0.5 \leq \alpha \leq 1.0$
- The target matching frequency, f_m, in the range $0.2 \leq f_m \leq 1.0$

Considering variations in the elastic scattering coefficient, η_S, ground-motion amplitudes for PGA and spectral acceleration at short periods varied by at most ±10 %, but generally stayed within ±5% from the values for $\eta_S \leq 0.03$ (consistent with findings of Mena et al, 2010). A similar variation is achieved simply by using different random-number seeds for generating the stochastic wavelets. The attenuation Q_0, representing the average crustal attenuation, was changed according to the findings by Edwards et al. (2009) and within a range of Q-values given in the literature. For Q_0 lower than about 300, the amplitude-versus-distance decrease of ground-motions is too rapid, leading to strong under-predictions at larger distances. We thus do not further consider $Q_0 < 300$. Values of $Q_0 \geq 500$ provided reasonable amplitude-distance decay; increasing Q_0 above 700 resulted in ground-motion amplitudes consistent with ground-motion prediction equations (e.g. Akkar & Bommer, 2010), while further increasing Q_0 to 1300 (Edwards et al, 2009) amplified the high-frequency motions only by 2-3 %. For internal consistency we select $Q_0 = 1300$ for our final set of simulations.

The implementation of the multiple-scattering theory (Zeng et al., 1991; Zeng, 1993) only considers the wave-amplitude attenuation due to elastic wave-scattering in a heterogeneous medium. To account for anelastic (intrinsic) attenuation, the common model of a frequency-dependent path-attenuation $Q(f) = Q_0 f^{\alpha}$ is used (e.g. Anderson and Hough, 1984; Atkinson and Silva, 1997), with the frequency-decay parameter α. In the corresponding literature a range of α-values is discussed, where $0 \leq \alpha \leq 1$, and the value of being regional dependent. Common values for the decay parameter are $0.5 \leq \alpha \leq 0.8$. We tested a range of values, but did not find very strong effect on ground-motion amplitude, aside from slide amplitude decrease for lower values of α. We thus use $\alpha = 0.7$ in our simulations, consistent with Atkinson and Silva (1997) and Mena et al. (2010).

Our broadband approach requires the definition of a target matching frequency. In most schemes for hybrid broadband computations (e.g. Graves and Pitarka, 2004), this transition frequency is fixed (e.g. to $f_m = 1$Hz) with the notion that wave-propagation in heterogeneous Earth is to a large extent deterministic at frequencies below 1 Hz, and tends to be increasingly stochastic at frequencies above 1Hz. Several studies report the loss (or at least a strong decrease) of directivity effects at frequencies above 1 Hz (e.g. Spudich and Chiou, 2008; Pulido and Kudo, 2004). In our simulation we assume a planar fault and a one-dimensional velocity-density profile, resulting in strong directivity effects due to the relative smoothness and coherence of the rupture evolution and the simplified wave-propagation. In nature, complex faulting geometry as well as heterogeneous Earth structure contribute to the breakdown of rupture coherency, which decreases directivity effects and increases high-frequency radiation.

We thus base the matching frequency on an estimate of the corner frequency of each individual rupture model in our set of 360 simulated events. For smaller earthquakes, that have higher corner frequencies, the matching frequency would also be higher, reflecting the fact of the generally increased high-frequency content of smaller earthquakes. The approximate corner frequency f_c is computed using the circular-rupture, constant stress-drop, fixed rupture-speed model of Brune (1970), $f_c = 0.42 \cdot \beta \cdot \left(\Delta\sigma / M_0\right)^{1/3}$

where β is the shear-wave speed at the source (in our case hypocenter) and Δσ is the average stress-drop over the effective rupture area. A number of tests revealed that $f_m = 3\ f_c$ as matching frequency provided consistent results with respect to the GMPEs; we find a minimum $f_m \sim 1.0$ Hz for the smallest events in our database of simulated events ($M_w \sim 5.7$) and a maximum $f_m \sim 0.2$ Hz for the largest scenario ruptures (an $M_w \sim 7.1$).

BROADBAND WAVEFORMS & GROUND-MOTION COMPARISONS

Ground-motion parameters computed from the broadband time histories are peak-ground acceleration (PGA), peak-ground velocity (PGV), and spectral acceleration, SA_T, at a range of periods, T. Response spectral values were computed with the Newmark-method for linear systems for the two horizontal components of motion (fault-normal Y, and fault-parallel X). For each GMP, we report the value of the geometric mean of the two horizontal components, computed as $GMP = \sqrt{GMP_X \cdot GMP_Y}$. For each scenario event we

apply site-amplification corrections to properly scale synthetics from the minimum shear-wave speed of 2500 m/s used in the dynamic calculations to a more typical Vs_{30}-values of 1500 m/s. The site-amplification corrections use period-dependent amplification coefficient of Borcherdt (1994; 2002), applied to the Fourier-amplitude spectrum of the simulated waveforms (Graves and Pitarka (2004). Note that we adopt Vs_{30} = 1500 m/s for site-correction instead of a more common value of 760 m/s (or even lower) since the applicability of the Borcherdt-approach to such strong alterations is not well tested. However, scaling to such low Vs_{30} would provide an additional amplitude increase of about a factor 1.2 – 1.5.

The intention of this study is not to deliver a set of waveforms for immediate engineering use, but rather to examine to what extent the current dynamically constrained broadband simulations are consistent with empirical predictions. If the simulations are generally in agreement with the empirical predictions, but show deviations from GMPE's or specific characteristics in the distance range of sparse observations (i.e. in the very near-source region), then future near-source ground-motion may be more adequately estimated using simulations rather then empirical predictions. For the following discussion it is important to note that we have made no attempt to optimize our parameterizations to match any empirical equation. All simulations are done with the same scattering-parameter set and site-amplification factors

Figure 3 displays two representative examples of broadband time series, their amplitude spectra, and the resulting geometric mean of spectral acceleration. As can be seen, the broadband time series exhibit a strong signature of the high-frequency scattering, which is evident also in the amplitude spectra that decay as 1/frequency above the matching frequency (f_m ~ 0.2-3 Hz in Figure 3), and out to ~50 Hz. However, the response-spectral characteristics, here compared in terms of the geometric mean, do not necessarily match the empirical predictions, despite the amplitude spectra appear to be "complete" in their frequency content.

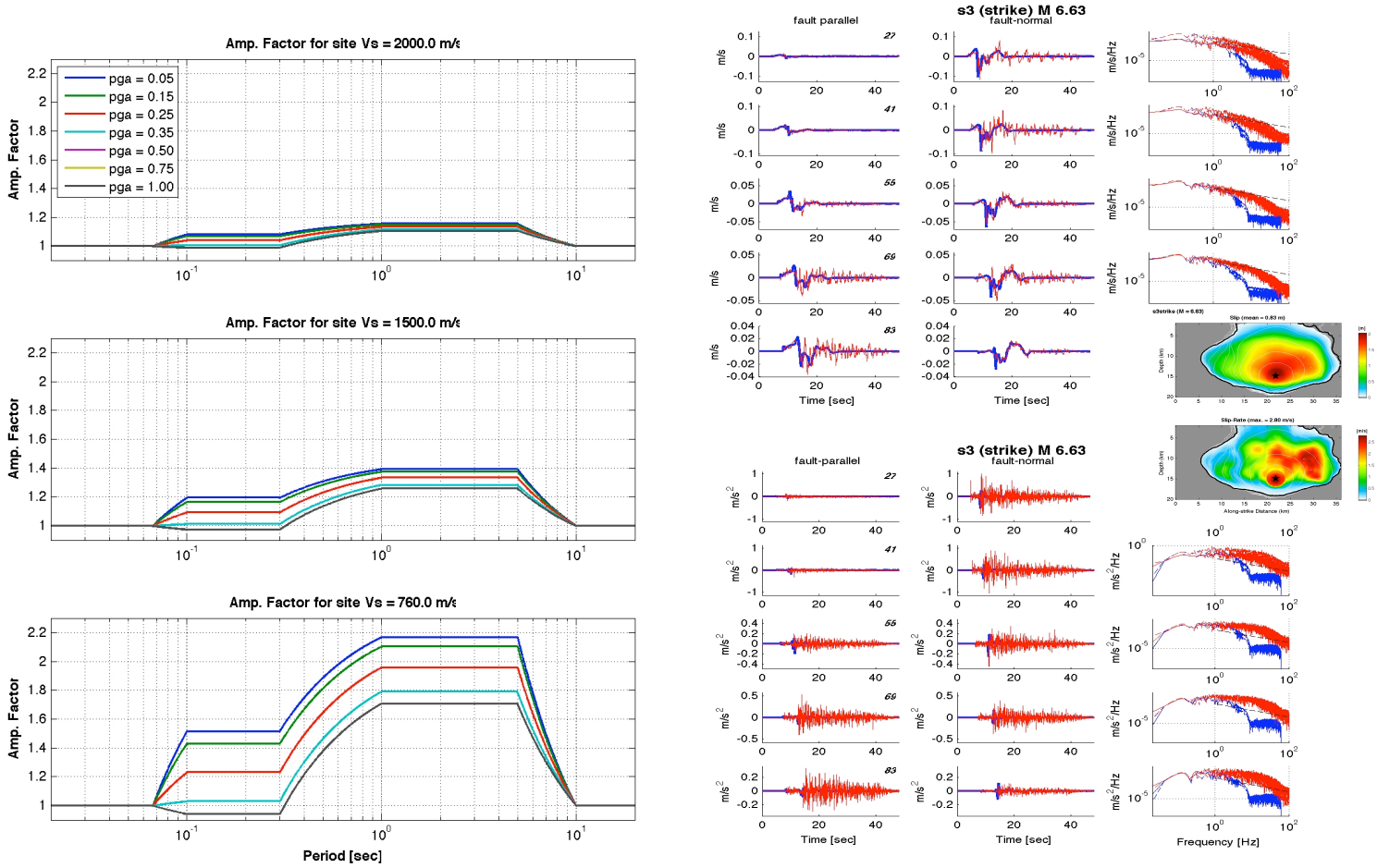

Figure 2: (Left) Site-amplification factors (Borcherdt, 1994; 2002) for different input PGA (colored lines) to scale ground-motions from input site Vs_{30} of 2500 m/s to Vs_{30} = 2000 m/s (top), Vs_{30} = 1500 m/s (center), and Vs_{30} = 760 m/s (bottom). (Right) Example hybrid broadband waveforms for a buried M 6.63 strike-slip earthquake, in terms of velocity (top) and acceleration (bottom) for five tstations at increasing distance from the fault. Broadband time series and amplitude spectra (right-most column) are plotted in red, low-frequency synthetics from dynamic calculations are shown in blue (inset: slip and slip-velocity on the fault for this event).

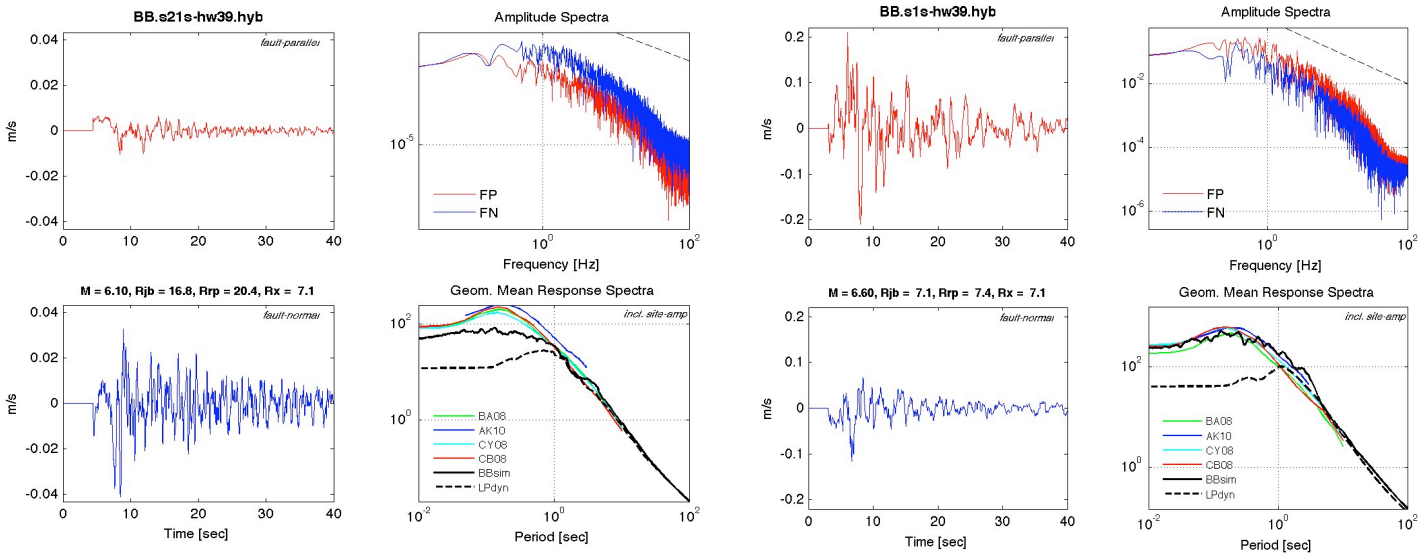

Figure 3: (Left) Fault-parallel (top-left) and fault-normal (bottom-right) ground-motion for an M_w 6.1 strike-slip rupture at ~ 16 km distance. The velocity-amplitude spectra (top-right) display an approximate 1/f decay up to ~50Hz. The broadband spectral response roughly matches empirical prediction (bottom-right), while the LF-response spectra cannot match the short periods. (Right) Same as left panels, but for an M_w 6.6 event at ~7km distance. In this case, the resulting spectral response matches the empirical predictions.

In the following, we compare selected parameters for a set of scenarios or sites, instead of individual waveforms or response spectra. Figure 4, for instance, shows ground-motion parameters for a buried M_w 6.62 strike-slip scenario given in Dalguer and Mai (2011; this volume; their Figure 3), compared with the empirical predictions by Boore & Atkinson (2008) and Akkar & Bommer (2010). Figure 5 displays ground-motions resulting from the same heterogeneous stress field, but now allowed to break the free surface. The corresponding rupture has increased magnitude, M_w 6.75, and therefore also larger shaking levels. In both cases, the simulation data follow the same distance-decay as the empirical curves predict. Shaking levels are generally in good agreement with the GMPE's, but weakly suggestive of higher-than-empirically-predicted variability. A similar pattern can be seen in Figure 6 which shows the resulting motion for the same initial stress distribution, but resolved on a 45°-dipping fault, generating an M_w 7.04 surface-breaking reverse-faulting earthquake.

Generally, we find that for a given random initial stress field in the dynamic calculations, the surface-breaking earthquakes have higher magnitude than the buried events, owing to the increased slip in the shallow parts of the fault. Moment magnitudes for the strike-slip and normal events are comparable, while the magnitudes of the thrust-faulting events are consistently 0.2-0.3 magnitudes higher. Adding to the magnitude difference the general pattern of larger ground-motions for reverse-faulting events (compared to strike-slip and normal faulting earthquakes) for the same magnitude, we find that – for identical initial random stress on the fault – the thrust-faulting ruptures will have considerably higher shaking levels than the strike-slip and normal-faulting ruptures.

To further analyze our simulation data, we plot ground-motions obtained from multiple events within a given magnitude bin (Figure 7 and 8), grouping ruptures within $M \pm \Delta M$, where $\Delta M = 0.1$, and their corresponding SA, PGA, and PGV values. Comparisons are made with respect to GMPE's for the center magnitude M, hence considerable under- and over-predictions are expected. We choose to compare against GMPE's that ignore higher-order parametrizations (e.g. hanging-wall/foot-wall effects; specific distance/location metrics), and only consider magnitude, Joyner-Boore distance, Vs30-value (here set to Vs30 = 1500 m/s) and faulting style. Because we opt for these simplifications we refrain from conducting a formal misfit- or bias-analysis of our simulations. The goal of this work is not to fit and reproduce the data of a specific (past) earthquake or prove/disprove the prediction of specific GMPE's. Rather, we want to test whether or not our hybrid broadband ground-motion simulation scheme based on spontaneous dynamic rupture models with random initial stress provide a viable method for realistic and accurate near-field ground-motion simulations.

Figure 7 and 8 show that the overall ground-motion level for the buried and surface-rupturing events agrees with the empirical predictions. For strike-slip events, many close-to-nodal sites display expected low shaking (marked by red crosses). Additionally, we find an indication for reduced motions (compared to GMPE's) at very close distances ($R_{JB} < 3$ km), which is most pronounced for buried strike-slip scenarios. While the distance decay of our simulations is consistent with the GMPE's, we find that the ground-motion variability in our results appears to exceed the uncertainties given in the GMPE's. This will be examined further below.

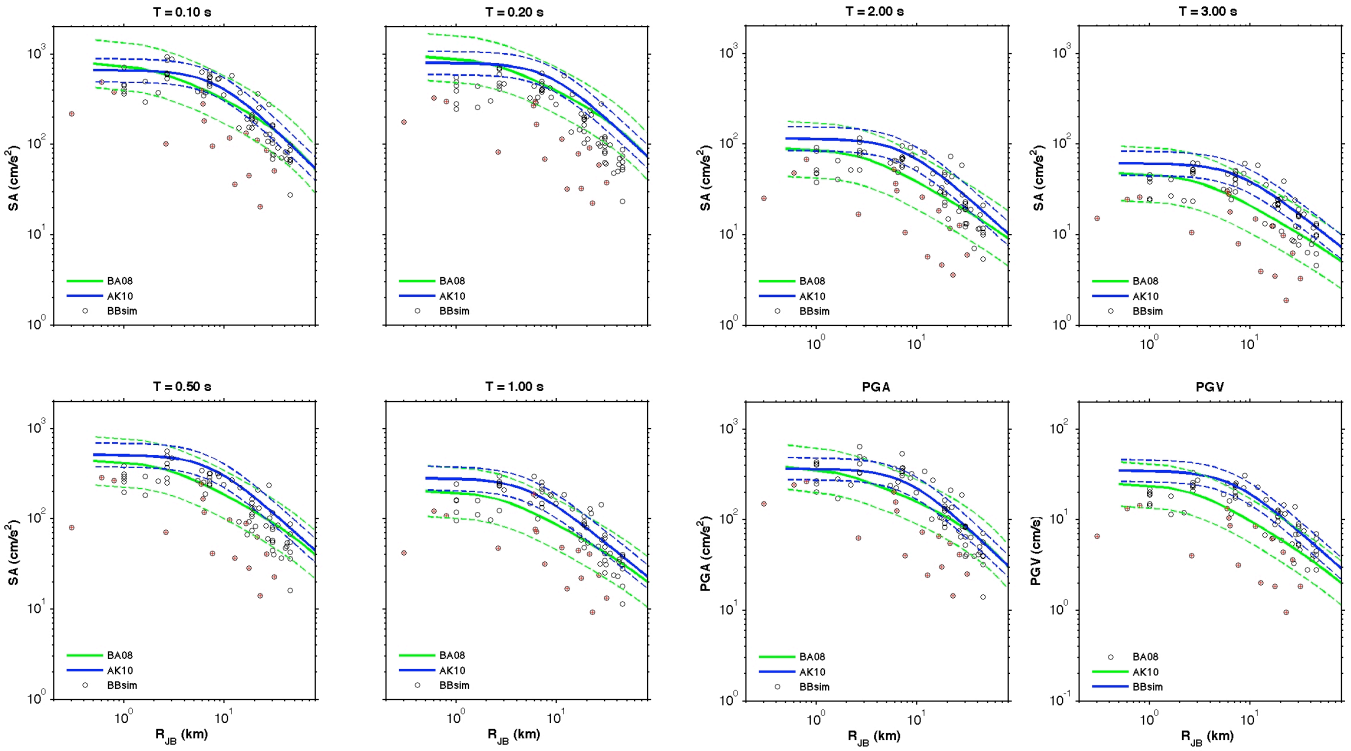

Figure 4: Ground-motion parameters for a buried M_w 6.62 strike-slip scenario earthquake, compared to the GMPE's by Akkar and Bommer (2010; blue) and Boore and Atkinson (2008; green). Dotted lines mark the ±1σ bounds. Simulation-data points marked with a red-cross are close-to nodal for strike-slip ruptures, and often have low ground-motions. R_{JB} is Joyner-Boore distance.

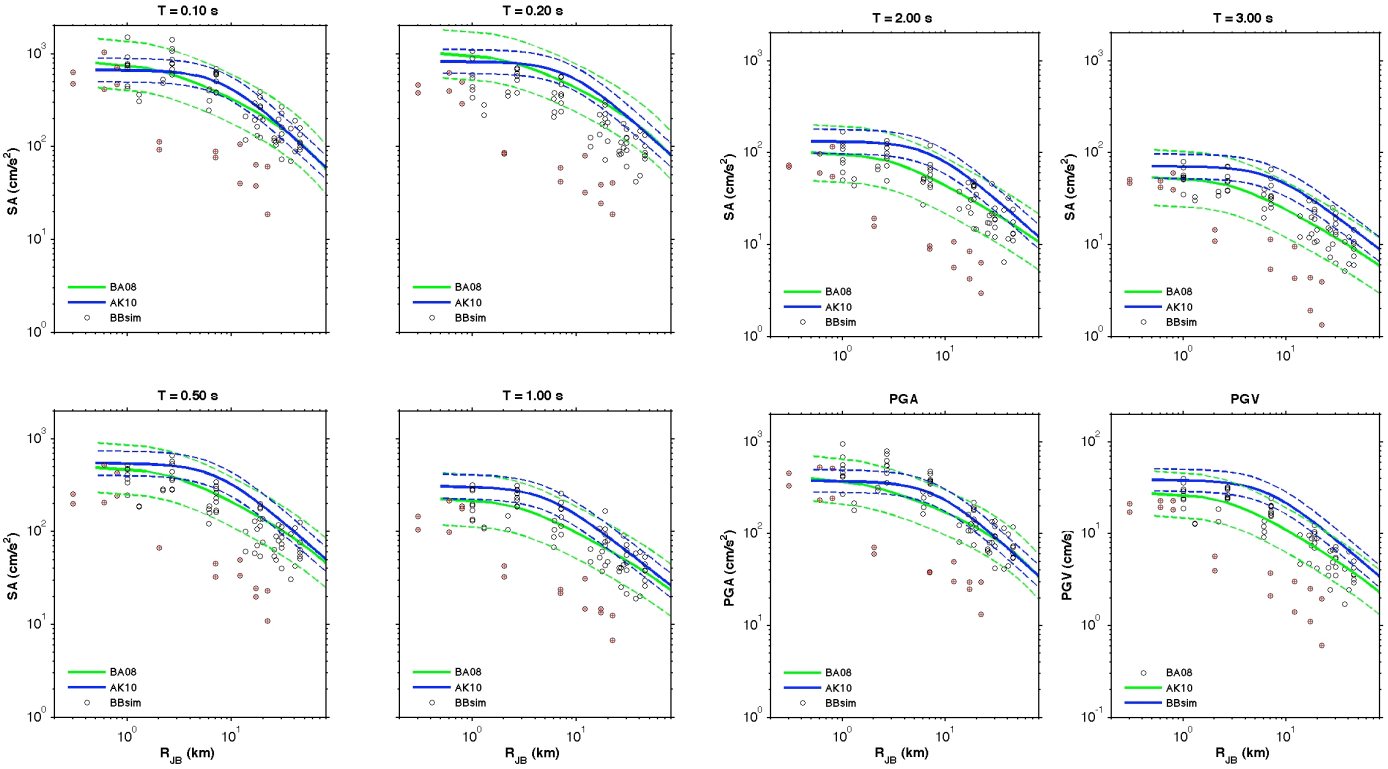

Figure 5: Same as Figure 4, for an M_w 6.75 strike-slip scenario earthquake that breaks the Earth surface.

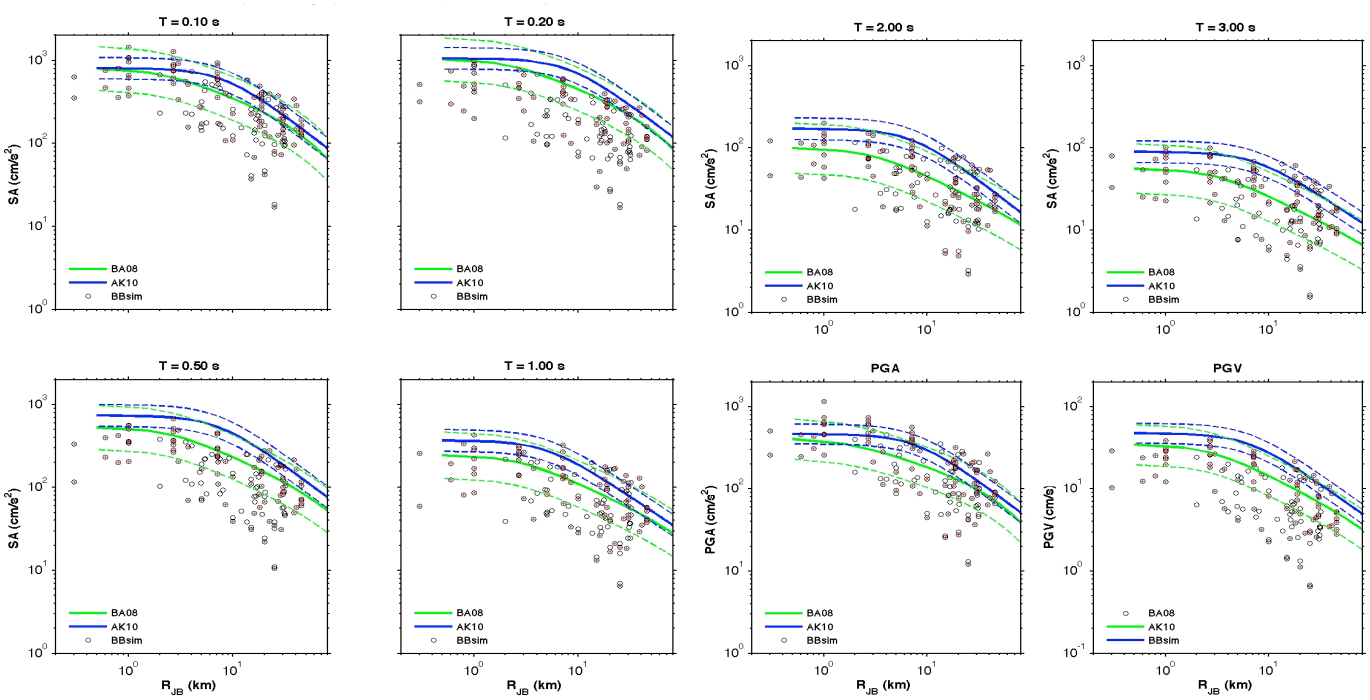

Figure 6: Same as Figure 4, for an M_w 7.04 reverse-faulting scenario earthquake that breaks the Earth surface. This dynamic rupture model for this scenario event has the same initial random stress field as the events shown in Figure 4 and 5 (see also Dalguer & Mai, 2011; this volume, and their Figures 3-5). Red crosses mark the foot-wall sites for this event.

Finally, we examine the resulting variability of the hybrid broadband ground-motions. Figure 9 displays σ_{lnY}-values against distance for a range of SA(T) as well as PGA and PGV from our simulations. To facilitate the analysis we group sites into distance bins of R_{JB}: [0.2 – 1.0] km; [1.0 – 2.5] km; [2.5 – 5.0] km; [5.0 – 10.0] km, [10 – 20] km, [20 – 35] km, and [35-50] km. We notice that ground-motion variability is generally close to $\sigma_{lnY} = 0.5$, oscillating between $\sigma_{lnY} = 0.4$ to $\sigma_{lnY} = 0.7$, with only mild dependency of σ_{lnY} on the distance. Normal-faulting and strike-slip ruptures exhibit a very similar behavior (as in the ground-motions themselves), while the variability for reverse-faulting events appears to be slightly lower. We do not find evidence for any magnitude dependence of ground-motion variability, but this could be due to the limited range in magnitude and fault dimensions in our calculations. Interestingly, we observe a small increase in σ_{lnY}-values for surface-rupturing events, potentially associated to the particular location of sites with respect to where the surface rupture occurs. For buried events, even the sites with smallest R_{JB}-distance are located a certain physical distance away from fault areas of large slip (moment-release); this is not the case for surface-rupturing events, and it is expected that sites of extreme motions are located close to surface-breaking areas or in regions of enhanced on-fault directivity (Mena and Mai, 2010).

CONCLUSIONS & DISCUSSION

We have carried out spontaneous dynamic rupture simulations for vertical strike-slip, 60°-dipping normal-faulting, and 45°-dipping thrust-faulting earthquake scenarios that either remain buried or are allowed to break the free surface, with depth-dependent or constant normal stress, resulting in a total of 360 source models. For this paper, long-period ground-motions were extracted at 84 (168 for thrust and normal faulting) locations for the models with depth-dependent normal-stress, and combined with high-frequency scattering Green's function to form physics-based broadband near-field seismograms. In total, we have generated over 25'000 three-component seismograms, which we then examined in terms PGA, PGV, and spectral acceleration at various periods, comparing with ground-motion prediction equations by Akkar & Bommer (2010) and Boore & Atkinson (2008).

Our findings indicate that the dynamically constrained broadband motions are in general consistent with the empirical prediction, but that they fail to exactly reproduce the GMPE values, but they capture correctly the overall characteristics of the predicted motions. Part of the discrepancy is due to incomplete accounting for local site amplification, however, we decided not to take the Borcherdt (1994) method to the extreme by scaling from Vs_{30} = 2500 m/s down to Vs_{30} = 760 m/s. Hence, simulated spectral-response values could be a factor ~1.5 larger. Another factor affecting ground-motion amplitudes is the relative simple one-dimensional velocity-density model (no 3D effects). Moreover, our comparisons use relatively simple GMPE's (in terms of parameterization), and refined

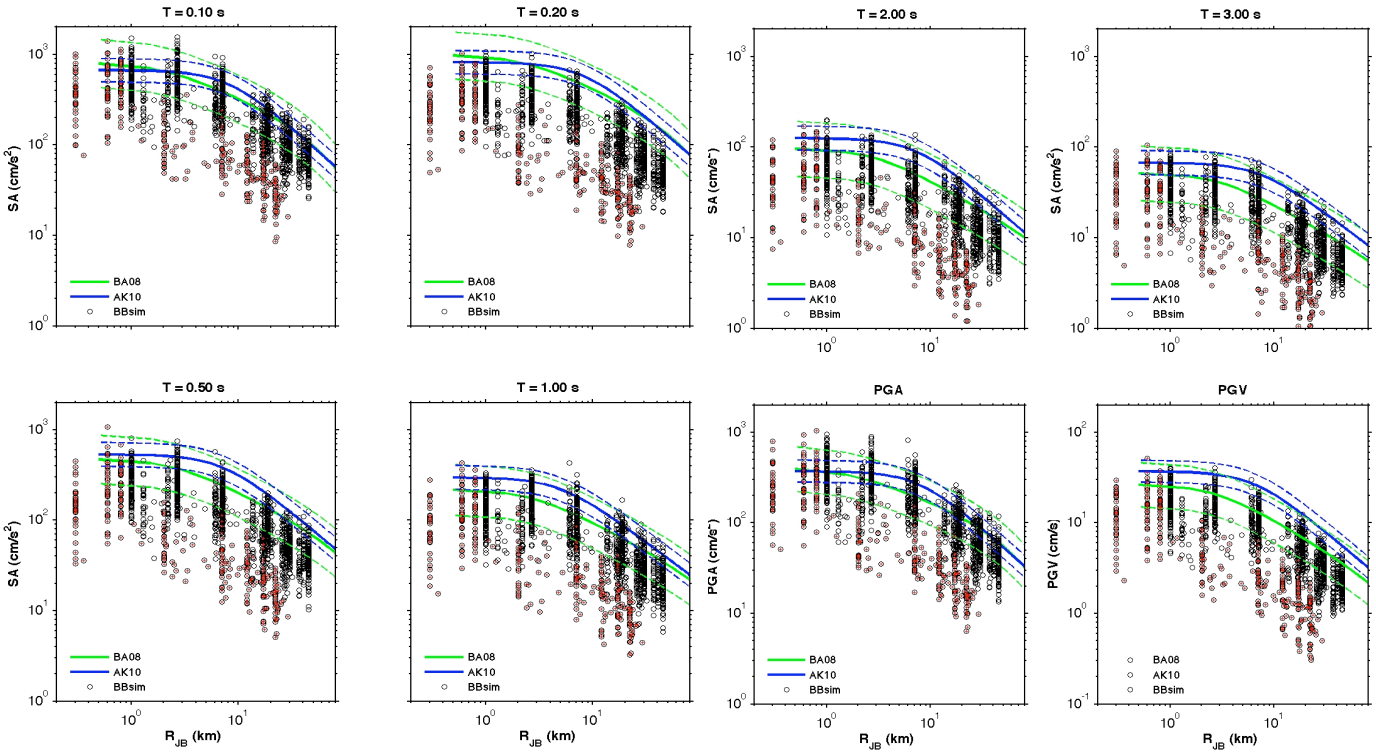

Figure 7a: Ground-motions parameters from hybrid broadband simulations of 19 surface-rupturing strike-slip events in the magnitude range $6.6 \leq M_w < 6.8$. Note that the GMPE's shown here were computed using the center magnitude M_w 6.7, and thus deviations between simulation-data and the empirical relations are expected to be larger than in Figures 4-6. Red crosses mark close-to-nodal stations (i.e. their fault-normal distance from surface projection of top-fault-edge is1 km or less).

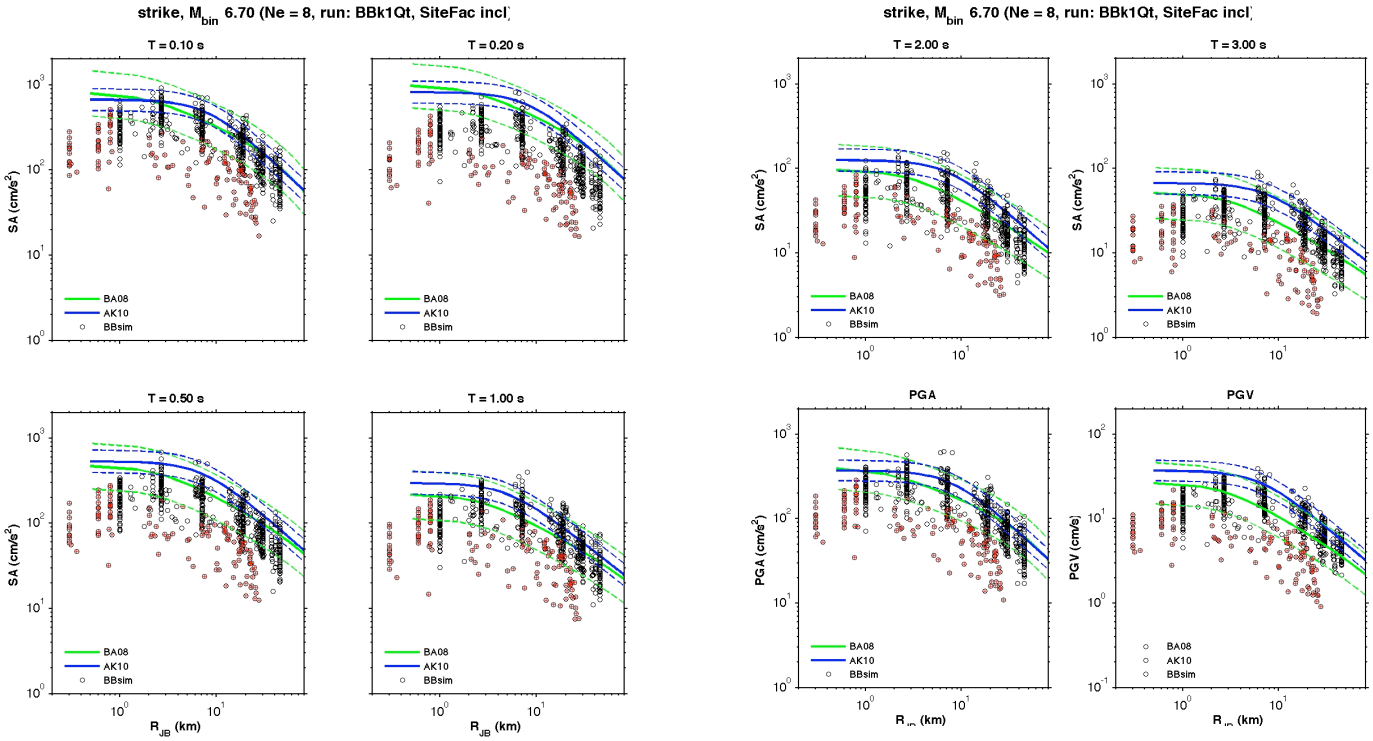

Figure 7b: Same as Figure 7a, but for 8 buried strike-slip events in the range $6.6 \leq M_w < 6.8$. Note the good agreement between non-nodal simulation data and the GMPE's at distances R_{JB} larger than about 3 km; note also the apparent ground-shaking decrease at very short distances ($R_{JB} < 3$ km) and the apparent larger ground-motion variability (at all distances).

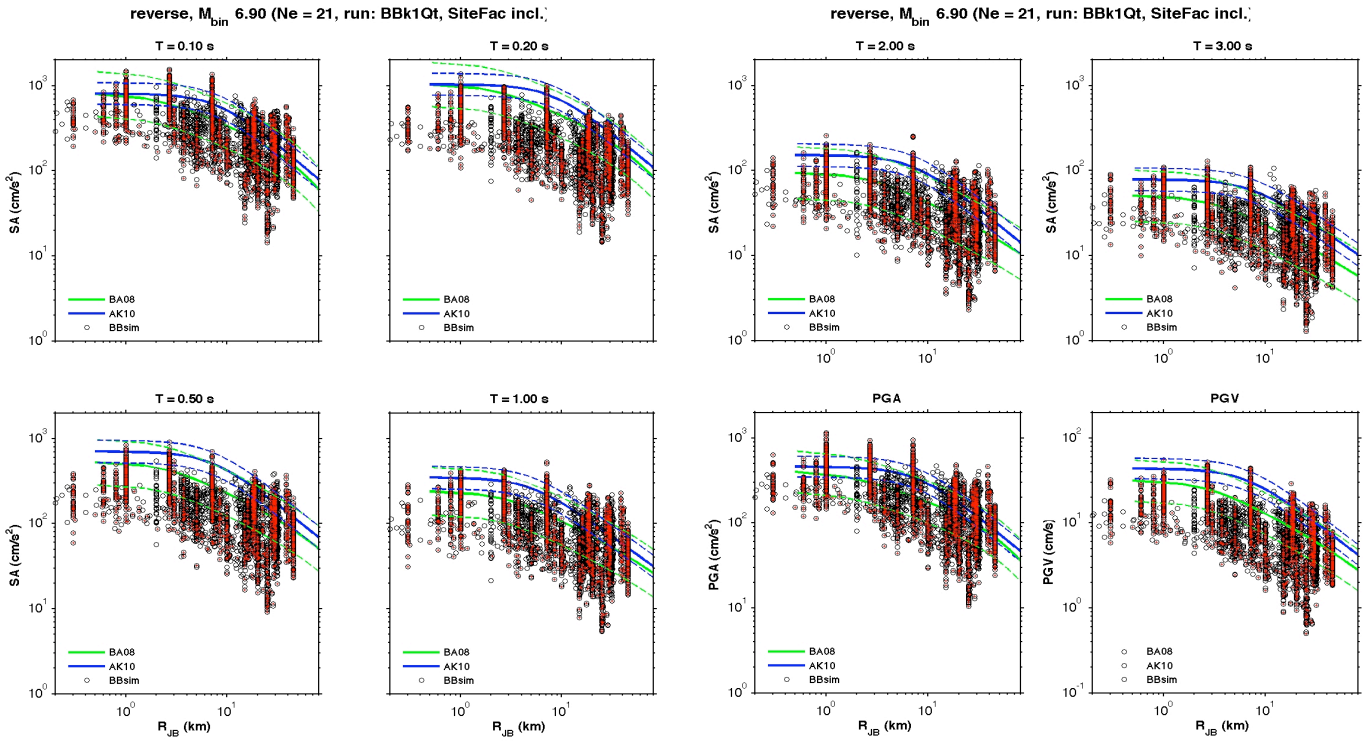

Figure 8a: Same as Figure 7a, but for 21 surface-breaking reverse-faulting events in the range $6.8 \leq M_w < 7.0$. Red crosses mark sites on the fault-wall for each event.

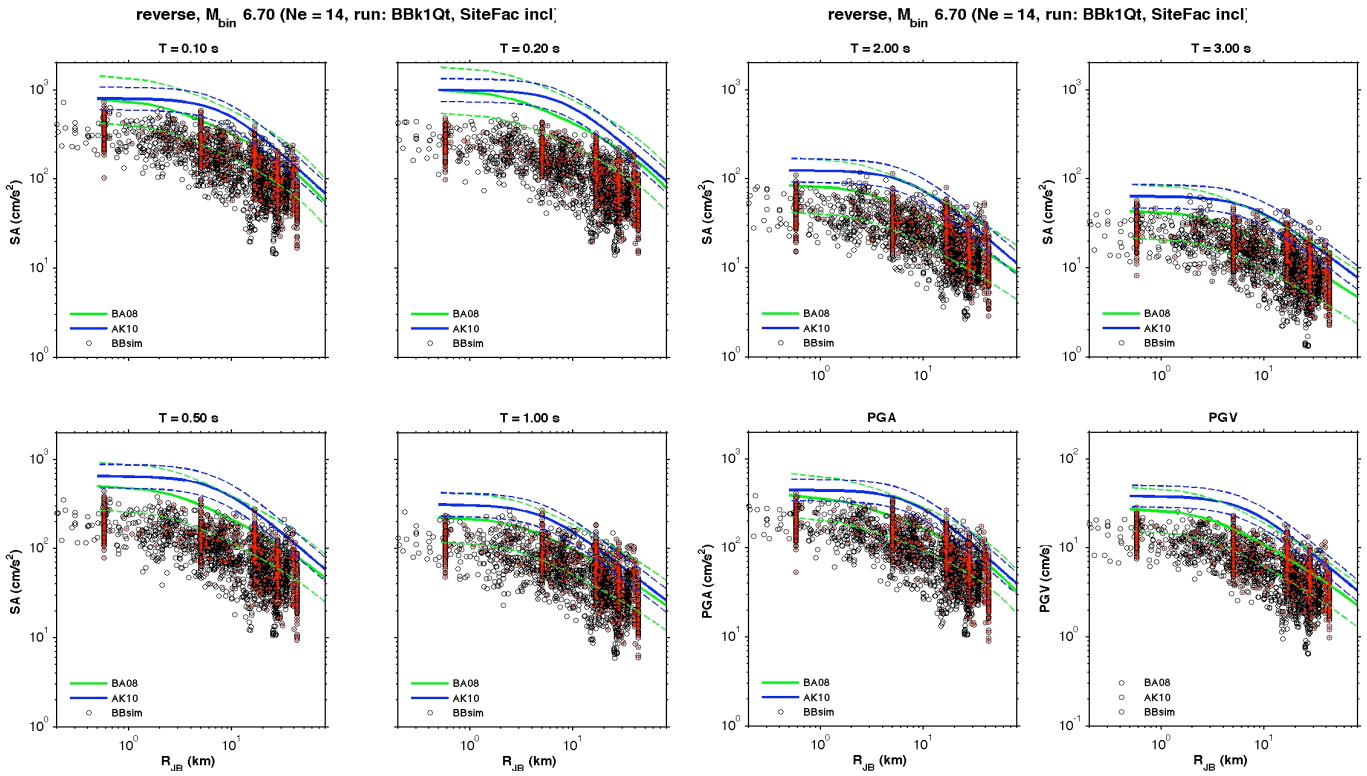

Figure 8b: Same as Figure 8a, but for 14 buried reverse-faulting events in the range $6.6 \leq M_w < 6.8$.

GMPE's may provide a different image. In particular the depth-to-top of the rupture is not accounted for in these GMPE's, despite its large effect on near-source ground-motion. Note also that when plotting ground-motion values against distance-to-rupture, R_{rup}, instead of Joyner-Boore distance, R_{jb}, the mismatch decreases since R_{rup} is a fundamental, physics-based distance measure. It is worth noting that the standard deviation from the numerical simulations is close to the empirically derived standard deviations.

Further work will consider dynamic rupture models that are less "crack-like", and are characterized by "patchier" slip distributions and more variable rupture propagation. This could potentially be achieved by different initial stress distributions. However, spatial variability of the slip-weakening distance and in particular non-planar fault geometry are better candidates to increase the roughness of the dynamic rupture models. Increased rupture complexity will radiate more effectively in the intermediate frequency range 0.3 – 3 Hz which is currently slightly too weak (i.e. the spectral decay in this range is faster than a 1/f decay). It is important to note that this frequency range has to be radiated by the source to ensure its proper radiation pattern which is assumed to transition from double-like radiation to isotropic radiation in the frequency range 1-4 Hz (Pulido and Kudo, 2004; Spudich and Chiou, 2008). The high-frequency scattering contribution is inherently isotropic, and hence cannot fully represent the radiation-pattern properties in the frequency range 0.3 – 3 Hz. Nevertheless, our hybrid broadband ground-motion simulation approach based on spontaneous dynamic rupture models has the potential to provide realistic time series for earthquake-engineering and seismic hazard purposes.

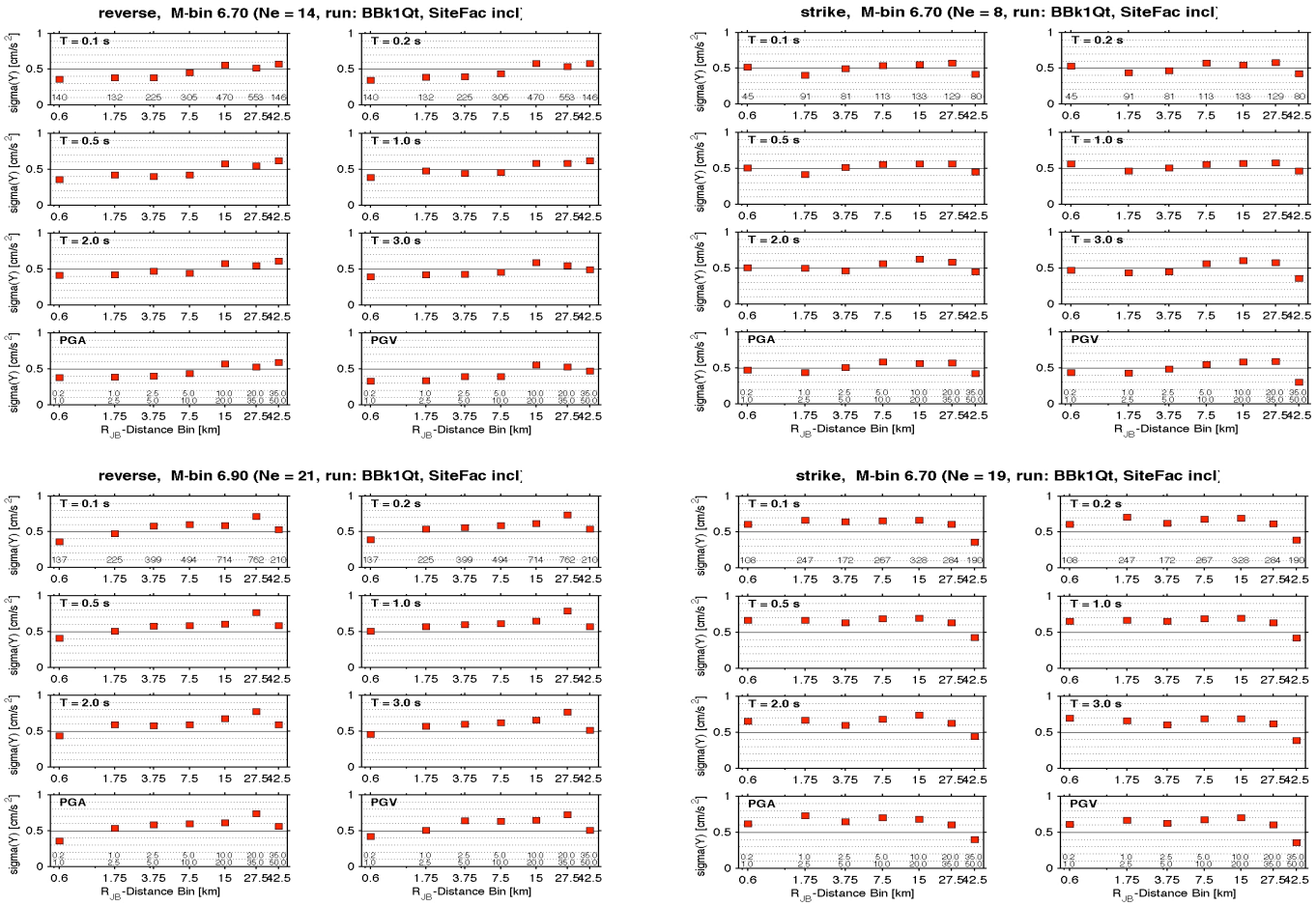

Figure 9: Ground-motion variability σ_{lnY} over distance, binned into seven distances ranges, for reverse (left column) and strike-slip (right column) events, comparing buried ruptures (top) against surface-rupturing events (bottom). See text for details.

REFERENCES

Anderson, J.G., and S.E. Hough (1984). A model for the shape of the Fourier amplitude spectrum of acceleration at high frequencies, Bull. Seism. Soc. Am., 74, 1969-1993.

Atkinson, G. M., and W. Silva (1997). An empirical study of earthquake source spectra for California earthquakes, Bull. Seismol. Soc. Am. 87, 97–113

Berge, C., Gariel, J.-C., Bernard, P., 1998. A very broad-band stochastic source model used for near source strong motion prediction. Geophys. Res. Lett. 25 (7), 1063–1066

Boore DM (1983) Stochastic simulation of high frequency ground motions based on seismological models of the radiation spectra. Bull Seismol Soc Am73:1865–1894

Borcherdt RD (1994) Estimates of site-dependent response spectra for design (methodology and justification). Earthquake Spectra 10(4):617–653

Borcherdt RD (2002) Empirical evidence for acceleration-dependent amplification factors. Bull Seis Soc Am. 92(2):761–782

Brune, J. N. (1970). Tectonic stress and the spectra of seismic shear waves from earthquakes, J. Geophys. Res. 75, 4997–5009

Dalguer, L.A. and M. Mai (2008), Implications of Style-of-Faulting and Loading Characteristics on the Dynamic Rupture Process, Eos Trans. AGU, 89(53), Fall Meet. Suppl., Abstract S51D-1798

Dreger, D., E. Tinti, and A. Cirella (2007), *Seismological Society of America 2007 Annual Meeting,* 11-13 April 2007

Edwards, B, D. Faeh, B. Allmann, and V. Poggi (2009). Stochastic ground-motion model for Switzerland, *Internal report submitted to the Pegasos Refinement Project Nov. 30, 2009*.

Graves, R, and A. Pitarka (2004), Broadband time history simulation using a hybrid approach, 13th World Conference on Earthquake Engineering, Vancouver, BC Canada, August 1-6, 2004, Paper No. 1098.

Graves, R.W. and A. Pitarka (2010), Broadband Ground-Motion Simulation Using a Hybrid Approach, Bull. Seis. Soc. Am., Vol. 100, No. 5A, pp. 2095–2123, October 2010, doi: 10.1785/0120100057

Guatteri, M., P.M. Mai, G.C. Beroza, and J. Boatwright (2003). Strong-ground motion prediction from stochastic-dynamic source models, *Bull. Seis. Soc. Am.*, Vol. 93 (1), pp. 301-313.

Hough, S.E., and J.G. Anderson (1988). High-frequency spectra observed at Anza, California – Implications for Q-structure, Bull. Seis. Soc. Am., Vol 78, 692-707

Mai, P.M.,G.C. Beroza (2000). Source-scaling properties from finite-fault rupture models, *Bull. Seis. Soc. Am.*, Vol. 90, pp. 604-615.

Mai, P.M., and G.C. Beroza (2002). A spatial random-field model to characterize complexity in earthquake slip, *J. Geophys. Res.*, Vol. 107 (B11), 2308, doi:10.1029/2001JB000588.

Mai, P.M., and G.C. Beroza (2003). A hybrid method for calculating near-source broadband seismograms: application to strong motion prediction, *Phys. Earth Planet. Int*., 137, 183-199

Mai, P.M. (2009) Ground Motion: Complexity and Scaling in the Near Field of Earthquake Ruptures, in *Encyclopedia of Complexity and Systems Science*, W.H.K. Lee and R. Meyers (Eds.), Springer, *pp 4435-4474.*

Mai, P.M., W. Imperatori, and K.B.Olsen (2010). Hybrid Broadband Ground-Motion Simulations: Combining Long-Period Deterministic Synthetics with High-Frequency Multiple S-to-S Backscattering Bull. Seis. Soc. Am., Vol. 100, No. 5A, pp. 2124–2142, doi: 10.1785/0120080194

Mena, B., P.M. Mai, K.B. Olsen, M. Purvance, and J. Brune (2010). Hybrid Broadband Ground-Motion Simulation Using Scattering Green's Functions: Application to Large-Magnitude Events, Bull. Seis. Soc. Am., Vol. 100, No. 5A, pp. 2143–2162, doi: 10.1785/0120080318

Mena, B., and P.M. Mai (2011), Selection and quantification of near-fault velocity pulses owing to source directivity. Georisk, Volume 5, Issue 1, March 2011, pages 25-43.

Olsen, K., S.M. Day, L.A. Dalguer, J. Mayhew, Y. Cui, J. Zhu, V.M. Cruz-Atienza, D. Roten, P. Maechling, T.H. Jordan, D. Okaya and A. Chourasia (2009) ShakeOut-D: Ground motion estimates using an ensemble of large earthquakes on the southern San Andreas fault with spontaneous rupture propagation, Geophys. Res. Lett., 36, L04303, doi:10.1029/2008GL036832.

Pitarka A, Irikura K, Iwata T, Sekiguchi H (1998) Three-dimensional simulation of the near-fault ground motion for the 1995 Hyogo-ken Nanbu (Kobe), Japan, Earthquake. Bull Seis Soc Am88(2):428–440

Pitarka A, Somerville P, Fukushima Y, Uetake T, Irikura K (2000) Simulation of near-fault strong-ground motion using hybrid Green's function. Bull Seis Soc Am90(3):566–586

Pulido, N., and T. Kubo (2004), Near-fault strong motion complexity of the 2000 Tottori earthquake (Japan) from a broadband source asperity model, Tectonophys., 390 (1{4), 177{192.

Ripperger, J.; P. M. Mai and J.-P. Ampuero (2008) Variability of near-field ground motion from dynamic earthquake rupture simulations Bull. Seism. Soc. Am., 98 (3), 1207-1228; doi:10.1785/0120070076

Shakal AF, Haddadi HR, Huang MJ (2006) Note on the Very-High-Acceleration Fault Zone 16 Record from the 2004 Parkfield Earthquake. Bull. Seis. Soc. Am. 96(3):S119–S128

Spudich, P., and B. S. J. Chiou (2008), Directivity in NGA earthquake ground motions: Analysis using isochrone theory, Earthquake Spectra, 24 (1), 279{298, doi:10.1193/1.2928225

Wells, D. L., and K. J. Coppersmith (1994). New empirical relationships among magnitude, rupture length, rupture width, rupture area, and surface displacement, *Bull. Seism. Soc. Am.* 84, 974–1002.

Zeng YH, Su F, Aki K (1991) Scattering wave energy propagation in a random Isotropic scattering medium. 1. Theory J Geophys Res 96(B1): 607–619.

Zeng YH (1993) Theory of scattered P-wave and S-wave energy in a random isotropic scattering medium. Bull Seis SocAm 83(4):1264–12.